Quarkonium dissociation in perturbative QCD

Juhee Hong and Su Houng Lee
Department of Physics and Institute of Physics and Applied Physics, Yonsei University, Seoul 03722, Korea

(Received 26 November 2018; published 15 March 2019)

For weakly bound quarkonia, we rederive the next-to-leading order cross sections of quarkonium dissociation by partons that include the hard thermal loop (HTL) resummation. Our results calculated with an effective vertex from the Bethe–Salpeter amplitude reduce to those obtained by potential nonrelativistic QCD (pNRQCD) in the relevant kinematical limit, and they can be used in a wide temperature range applicable to heavy-quark systems in heavy-ion collisions. Based on the lattice computation of the temperature-dependent binding energy, our numerical analysis on $\Upsilon(1S)$ indicates that at high temperature the dominant mechanism for quarkonium dissociation is inelastic parton scattering as expected in the quasifree approximation, while it is gluo-dissociation at low temperature. By comparing with the momentum diffusion coefficient of a heavy quark, we discuss possible $O(g)$ corrections to the next-to-leading-order thermal width.

DOI: 10.1103/PhysRevC.99.034905

I. INTRODUCTION

Quarkonia are an important probe of high-temperature and -density matter produced in relativistic heavy-ion collisions. The suppression of quarkonia and their sequential melting provide information about the formation of quark-gluon plasma, the thermal properties of the matter, and the heavy-quark potential at finite temperature. Originally, color screening in deconfined quark-gluon plasma has been thought to prevent heavy quarks from forming a bound state [1]. Now quarkonia are believed to dissolve at high temperature not because the binding energy vanishes but because the thermal width becomes as large as the reduced binding energy.

Quarkonium suppression has been investigated for a long time, but their yields still need to be understood quantitatively. For recent reviews, see Refs. [2,3]. In addition to color-screening, quarkonia yields are affected by other mechanisms including Landau damping, feed-down, initial-state conditions, cold nuclear matter effects, and possible regenerations near the threshold. In this work, we focus on the dissociation mechanisms of quarkonia. We are especially interested in the ground state of bottomonium $\Upsilon(1S)$, since it survives at high temperature up to ∼600 MeV [3]. Recently, bottomonium suppression has been observed in Pb + Pb collisions at $\sqrt{s_{NN}} = 2.76,\ 5.02$ TeV by the CMS collaboration [4,5] and in U + U collisions at $\sqrt{s_{NN}} = 193$ GeV by the STAR collaboration [6].

From a partonic picture, there are two main mechanisms of quarkonium dissociation. The first is gluo-dissociation, $g + \Upsilon \to Q + \bar{Q}$, where Υ is quarkonium and $Q(\bar{Q})$ a heavy (anti)quark. Gluo-dissociation, also known as the thermal breakup of the heavy quark-antiquark color singlet state in effective-field theory, breaks the bound state by absorbing a gluon from thermal medium. The dipole interaction of color charge with a gluon [7,8] has been used to study the dissolution of quarkonia. The second mechanism is inelastic parton scattering, $p + \Upsilon \to p + Q + \bar{Q}$ with $p = g, q, \bar{q}$. This is related to the Landau damping phenomenon which results from scattering of hard particles in a thermal bath exchanging spacelike gluons. Quarkonium dissociation by inelastic parton scattering has been investigated in the quasifree approximation, where the reaction is taken care of by the sum of $p + Q \to p + Q$ and $p + \bar{Q} \to p + \bar{Q}$ [9]. For a tightly bound state near the phase transition, gluo-dissociation is an efficient process [7], while inelastic parton scattering is expected to be dominant when loosely bound quarkonia scatter with hard particles [2,9]. In an effective-field theory framework, inelastic parton scattering is also expected to be dominant at high temperature, but the quasifree approximation might overestimate the dissociation cross sections [10,11]. For this reason, we need to calculate inelastic parton scattering exactly and compare its contribution with that of gluo-dissociation.

Recently, there have been rigorous and formal developments in the calculations on these issues. The quark-antiquark static potential has been derived in finite-temperature QCD, where it has been found that the potential develops an imaginary part that results in the thermal width [12]. The real part of the potential is a screened Coulomb potential, and the imaginary part is induced by the Landau damping. Furthermore, in an effective-field theory framework another part of the imaginary potential has been found to arise by the singlet-to-octet thermal transition [13]. In different temperature regimes at weak coupling, potential nonrelativistic QCD (pNRQCD) has been used to study quarkonium dissociation [11,13–15].

While the low-energy effective-field theory is an important formal development, the various results valid at different energy and temperature scales are problematic when trying to continuously use them in realistic estimates for the fate of quarkonium. This is because the hierarchy of nonrelativistic and thermal scales varies during the time evolution in relativistic heavy-ion collisions, although the inverse of the typical distance between a heavy quark and antiquark is assumed to be larger than the binding-energy scale. Even in this short-distance limit, there is no universal picture with a single

interpolating formula that can be used throughout the entire evolution process. Moreover, since these imaginary parts of the potential are related to the two mechanisms of quarkonium dissociation, we might be able to obtain the resulting thermal width from the perspective of scattering processes ($g + \Upsilon \to Q + \bar{Q}$ and $p + \Upsilon \to p + Q + \bar{Q}$). Therefore, our aim is to introduce the partonic picture for quarkonium dissociation at short distance that reduces to the formal limit of the effective-field theory calculations at the relevant kinematical regime, but that can also interpolate between different temperature scales which are applicable to heavy-quark systems in evolving plasmas.

This work is organized as follows: In Sec. II, we discuss gluo-dissociation up to next-to-leading order. In Sec. III, we use an effective vertex derived from the leading order dissociation to calculate inelastic parton scattering which contributes to dissolution at next-to-leading order. In Sec. IV, we present a numerical analysis for weakly coupled $\Upsilon(1S)$ based on the lattice data of the temperature-dependent binding energy. In Sec. V, we discuss possible $O(g)$ corrections to the next-to-leading order thermal width. Finally, we summarize our results in Sec. VI.

II. GLUO-DISSOCIATION

In the heavy-quark limit, heavy-quark systems can be treated by using perturbative QCD with the interquark potential reducing to the Coulomb type. In Ref. [7], Peskin has calculated the interactions between partons and heavy-quark bound states by performing the operator product expansion on gluon insertions in the heavy-quark states. As an application, the gluo-dissociation cross section of quarkonium has been obtained at leading order [8], and later the same cross section has been rederived by using the Bethe–Salpeter amplitude [16]. In $1/N_c$ expansion in the large-N_c limit, the heavy-quark–antiquark pair after dissociation is noninteracting such that the dissolution is induced by the processes shown in Fig. 1 [and another similar to Fig. 1(a) but with P_1, P_2 exchanged].

For $\boldsymbol{q} \sim \boldsymbol{p}_1, \boldsymbol{p}_2 \gg \boldsymbol{k}$, the sum of the leading processes gives the following scattering amplitude [16]:

$$\mathcal{M}^{\mu\nu}_{\rm LO} = -g\sqrt{\frac{m_\Upsilon}{N_c}}\left[\boldsymbol{k}\cdot\frac{\partial\psi(\boldsymbol{p})}{\partial\boldsymbol{p}}\delta^{\mu 0} + k_0\frac{\partial\psi(\boldsymbol{p})}{\partial p^i}\delta^{\mu i}\right]\delta^{\nu j}\bar{u}(P_1) \times \frac{1+\gamma_0}{2}\gamma^j\frac{1-\gamma^0}{2}T^a v(P_2), \tag{1}$$

where $\psi(\boldsymbol{p})$ is the normalized wave function for a bound state with the relative momentum, $\boldsymbol{p} = (\boldsymbol{p}_1 - \boldsymbol{p}_2)/2$. The matrix element squared is

$$|\mathcal{M}|^2_{\rm LO} = \frac{8\left(N_c^2-1\right)}{N_c}g^2m^2m_\Upsilon k_0^2|\nabla\psi(\boldsymbol{p})|^2, \tag{2}$$

where we have used the transverse polarization $(\delta^{ij} - \hat{k}^i\hat{k}^j)$ for gluon. Dividing by the quarkonium polarization d_Υ and the gluon degeneracy $d_g = 2(N_c^2 - 1)$, the averaged scattering cross section is given by

$$\sigma_{\rm LO}(k) = \frac{1}{4\sqrt{(Q\cdot K)^2 - m_\Upsilon^2 m_k^2}}\int\frac{d^3\boldsymbol{p}_1}{(2\pi)^3 2p_{10}}\int\frac{d^3\boldsymbol{p}_2}{(2\pi)^3 2p_{20}} \times (2\pi)^4\delta^4(Q+K-P_1-P_2)\frac{1}{d_\Upsilon d_g}|\mathcal{M}|^2_{\rm LO}. \tag{3}$$

In the heavy-quark limit, the heavy-quark–antiquark pair is assumed to be weakly bound so that the leading order ground-state wave function of quarkonium can be described by the Coulombic bound state [7]:

$$|\nabla\psi_{1S}(\boldsymbol{p})| = 2^5\sqrt{\pi}\frac{a_0^{7/2}\boldsymbol{p}}{[(a_0\boldsymbol{p})^2+1]^3}, \tag{4}$$

where $a_0 = 16\pi/(N_c m g^2)$ is the Bohr radius. In the rest frame of the plasma where quarkonium is approximately at rest, we obtain [8,16]

$$\sigma_{\rm LO}(k) = \frac{2^7 g^2 a_0^2}{d_\Upsilon N_c}\frac{E^{7/2}(k-E)^{3/2}}{k^5}. \tag{5}$$

Here $E = 2m - m_\Upsilon > 0$ is the binding energy of quarkonium, and the relation $a_0^2 = 1/(mE)$ is satisfied for the Coulombic binding energy.

The thermal width of gluo-dissociation is related to the discontinuity, or the imaginary part, of the self-energy diagram of the quarkonium color singlet (see Fig. 4 without the hard thermal loop resummation) [17,18],

$$\mathrm{Im}\Pi_{\text{gluo-diss}} = -\frac{1}{2d_\Upsilon}\int\frac{d^4K}{(2\pi)^4}\int\frac{d^4P_1}{(2\pi)^4} \times 2\pi\delta(K^2)2\pi\delta\left(P_1^2-m^2\right) \times 2\pi\delta((Q+K-P_1)^2-m^2)|\mathcal{M}|^2_{\rm LO}n(k). \tag{6}$$

The relevant width is given by [19]

$$\Gamma_{\text{gluo-diss}} = \frac{1}{2d_\Upsilon q_0}\int\frac{d^3\boldsymbol{k}}{(2\pi)^3 2k_0}\int\frac{d^3\boldsymbol{p}_1}{(2\pi)^3 2p_{10}}\int\frac{d^3\boldsymbol{p}_2}{(2\pi)^3 2p_{20}} \times (2\pi)^4\delta^4(Q+K-P_1-P_2)|\mathcal{M}|^2_{\rm LO}n(k), \tag{7}$$

which, with Eq. (3), can be reexpressed by convoluting the cross section with a thermal distribution function of an incoming gluon [9]

$$\Gamma_{\text{gluo-diss}} = d_g\int\frac{d^3\boldsymbol{k}}{(2\pi)^3}\sigma(k)n(k). \tag{8}$$

Here, to break a bound state, the magnitude of an incoming gluon momentum is required to be larger than the binding energy, $|\boldsymbol{k}| \geqslant E$.

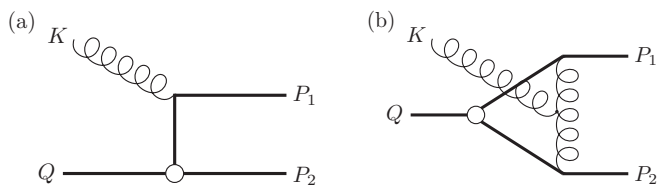

FIG. 1. The leading order gluon-quarkonium interactions. Thick solid lines denote quarkonium (Q) or heavy (anti)quarks (P_1, P_2), and wiggly lines are gluons.

To obtain the cross section and the thermal width at leading order, we have assumed that the external gluon is massless and $k \sim k_0 \gg m_D$. On the other hand, at finite temperature gluons acquire the thermal self-energy that leads to thermal mass $\sim m_D$. To accommodate such self-energy effects, we note that the phase space of the initial gluon involves the following on-shell condition for the leading-order dispersion relation:

$$1 = \int dk_0 \delta(k_0 - k) = \int dk_0 2k_0 \delta\left(k_0^2 - k^2\right), \tag{9}$$

which has been used in the leading-order computation. The δ function on the right-hand side of Eq. (9) corresponds to the leading-order spectral function of gluons which appears naturally when Eq. (8) is expressed in a covariant form. Using the covariant form, one can conveniently include the thermal effects at next-to-leading order, as discussed below.

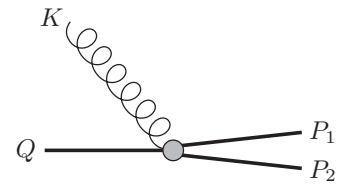

FIG. 2. The effective vertex derived from the sum of the leading processes shown in Fig. 1.

In the case of $k \ll T$ and $k_0^2 - k^2 \sim m_D^2$, the hard thermal loop (HTL) resummation is needed and the dispersion relation for transverse gluons is then given by

$$k_0^2 - k^2 - \mathrm{Re}\Pi_T(k_0, k) = 0. \tag{10}$$

In the Coulomb gauge, the HTL self-energies are [20]

$$\Pi_L(k_0, k) = m_D^2\left[1 - \frac{k_0}{2k}\ln\left(\frac{k_0 + k}{k_0 - k}\right)\right], \quad \Pi_T(k_0, k) = \frac{m_D^2}{2}\left[\frac{k_0^2}{k^2} - \frac{\left(k_0^2 - k^2\right)k_0}{2k^3}\ln\left(\frac{k_0 + k}{k_0 - k}\right)\right], \tag{11}$$

which do not have imaginary parts for timelike ($k_0^2 > k^2$) gluons. Therefore, at next-to-leading order, Eq. (9) is extended as follows:

$$\int dk_0 2k_0 \delta\left(k_0^2 - k^2 - \frac{m_D^2}{2}\left[\frac{k_0^2}{k^2} - \frac{\left(k_0^2 - k^2\right)k_0}{2k^3}\ln\left(\frac{k_0 + k}{k_0 - k}\right)\right]\right) \simeq \left\{1 + \frac{m_D^2}{4k^2}\left[\ln\left(\frac{8k^2}{m_D^2}\right) - 2\right]\right\}^{-1}, \tag{12}$$

where we have used $k_0 \simeq k$ and in the argument of the logarithm $k_0 - k \simeq \frac{m_D^2}{4k}$.

Through the definition of the thermal width given in Eq. (8), the next-to-leading order cross section for gluo-dissociation is derived by involving Eq. (12) in the leading-order result,

$$\sigma_{\mathrm{NLO}}(k) \simeq \left\{1 - \frac{m_D^2}{4k^2}\left[\ln\left(\frac{8k^2}{m_D^2}\right) - 2\right]\right\}\sigma_{\mathrm{LO}}(k), \tag{13}$$

where the effect of the relative velocity between quarkonium and gluon is included. If we neglect the final-state rescattering effects of the unbound heavy-quark–antiquark pair in the large-N_c limit, Eq. (13) agrees with the pNRQCD result [11,15] for the $mv \gg T \gg E \gg m_D$ case (in this regime, gluo-dissociation is the dominant dissociation mechanism in the effective-field theory framework).

III. INELASTIC PARTON SCATTERING

In this section, we introduce an effective vertex which is derived from the leading-order scattering processes of Fig. 1. In terms of the vertex, we calculate inelastic parton scatterings which contribute to quarkonium dissociation at next-to-leading order.

From the leading-order scattering amplitude of Eq. (1), the following effective vertex can be derived [21]:

$$V^{\mu\nu}(K) = -g\sqrt{\frac{m_\Upsilon}{N_c}}\left[\boldsymbol{k}\cdot\frac{\partial\psi(\boldsymbol{p})}{\partial\boldsymbol{p}}\delta^{\mu 0} + \left(\frac{\boldsymbol{p}^2}{m} + E\right) \times \frac{\partial\psi(\boldsymbol{p})}{\partial p^i}\delta^{\mu i}\right]\delta^{\nu j}\frac{1+\gamma^0}{2}\gamma^j\frac{1-\gamma^0}{2}T^a, \tag{14}$$

and denoted by Fig. 2. With the energy conservation, $\boldsymbol{p}^2/m + E \simeq k_0$ (k_0 is the energy transfer), this vertex is similar to the potential nonrelativistic QCD (pNRQCD) vertex. The difference is that our approach involves $1 \pm \gamma^0$ matrices because of the nonrelativistic treatment of heavy quarks, while in pNRQCD the octet propagator is employed to calculate the imaginary part of the potential. As will be shown below, our results agree with those by pNRQCD in a certain regime where inelastic parton scattering becomes dominant. The reason is that the rescattering effects in the octet propagator become

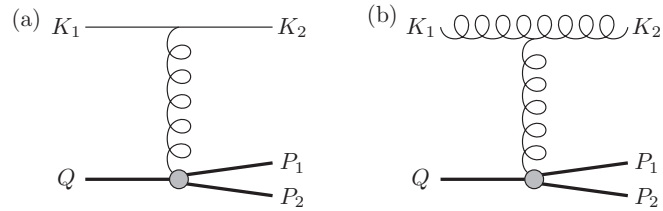

FIG. 3. The inelastic parton scattering processes which contribute to quarkonium dissociation at next-to-leading order (NLO). Panel (b) gives $O(g)$ corrections to the NLO thermal width if all the gluons are soft.

subleading and the chromoelectric dipole interaction can be taken into account through the effective vertex of Eq. (14). This vertex reflects the dipole interaction of color charge for the leading gluon-quarkonium interaction considered in Refs. [7,8].

For quarkonium dissolution by inelastic parton scattering, we consider barely bound quarkonia with near-threshold energy so that partons in a heat bath separate a heavy-quark–antiquark pair almost collinearly. In the quarkonium rest frame, the energy transfer is small ($k_{10} \simeq k_{20}$) and the only contribution is from the longitudinal gluon part of the effective vertex in Eq. (14). This situation is similar to that of the momentum diffusion of a heavy quark where the internal gluon attached to the Wilson line is longitudinal [22,23].

Inelastic parton scattering shown in Fig. 3 can be calculated by using the effective vertex. For $\boldsymbol{k}_1, \boldsymbol{k}_2 \gg \boldsymbol{k}_1 - \boldsymbol{k}_2$, the corresponding scattering amplitudes are given by

$$\begin{aligned}
\mathcal{M}^{\mu(q)}_{\rm NLO} &= g\bar{u}(K_2)\gamma_\nu T^a u(K_1)\frac{1}{(K_1-K_2)^2-\Pi(K_1-K_2)}\bar{u}(P_1)V^{\nu\mu}(K_1-K_2)v(P_2),\\
\mathcal{M}^{\mu\nu\lambda(g)}_{\rm NLO} &= -igf^{abc}\bar{u}(P_1)V^{\rho\mu}(K_1-K_2)v(P_2)\frac{1}{(K_1-K_2)^2-\Pi(K_1-K_2)}\\
&\quad\times\left[g^\nu_\rho(2K_1-K_2)^\lambda - g^\lambda_\rho(K_1-2K_2)^\nu - g^{\lambda\nu}(K_1+K_2)_\rho\right].
\end{aligned} \tag{15}$$

In the Coulomb gauge, the HTL propagator of longitudinal gluons is $i/[k^2+\Pi_L(k_0,k)] \simeq i/(k^2+m_D^2)$ for small energy transfer. The matrix elements squared are then

$$\begin{aligned}
|\mathcal{M}|^{2\,(q,\bar{q})}_{\rm NLO} &\simeq \frac{16N_f\left(N_c^2-1\right)}{N_c}g^4m^2m_\Upsilon|\nabla\psi(\boldsymbol{p})|^2\frac{(\boldsymbol{k}_1-\boldsymbol{k}_2)^2k_{10}^2}{\left[(\boldsymbol{k}_1-\boldsymbol{k}_2)^2+m_D^2\right]^2}\left[1+\frac{\boldsymbol{k}_1\cdot\boldsymbol{k}_2}{k_1k_2}\right],\\
|\mathcal{M}|^{2(g)}_{\rm NLO} &\simeq 16\left(N_c^2-1\right)g^4m^2m_\Upsilon|\nabla\psi(\boldsymbol{p})|^2\frac{(\boldsymbol{k}_1-\boldsymbol{k}_2)^2k_{10}^2}{\left[(\boldsymbol{k}_1-\boldsymbol{k}_2)^2+m_D^2\right]^2}\left[1+\frac{(\boldsymbol{k}_1\cdot\boldsymbol{k}_2)^2}{k_1^2k_2^2}\right],
\end{aligned} \tag{16}$$

where in the gluon-induced reaction we have used transverse polarizations for external gluons.

By integrating over the phase space and dividing by the initial flux, the dissociation cross section is obtained as

$$\begin{aligned}
\sigma_{\rm NLO}(k_1) &= \frac{1}{4\sqrt{(Q\cdot K_1)^2-m_\Upsilon^2m_{k_1}^2}}\int\frac{d^3\boldsymbol{k}_2}{(2\pi)^3 2k_{20}}\int\frac{d^3\boldsymbol{p}_1}{(2\pi)^3 2p_{10}}\int\frac{d^3\boldsymbol{p}_2}{(2\pi)^3 2p_{20}}\\
&\quad\times(2\pi)^4\delta^4(Q+K_1-K_2-P_1-P_2)\frac{1}{d_\Upsilon d_p}|\mathcal{M}|^2_{\rm NLO},
\end{aligned} \tag{17}$$

where d_p ($p = g$, q) is the degeneracy factor of the incoming parton. To perform the phase-space integration, we proceed as follows [24,25]: First, $\boldsymbol{p}_2$ integration is done by using the three-dimensional δ function, and $\boldsymbol{k}_2$ integration is changed to $\boldsymbol{k} = \boldsymbol{k}_1 - \boldsymbol{k}_2$. For the (anti)quark-quarkonium scattering, we have

$$\sigma^{(q,\bar{q})}_{\rm NLO}(k_1) \simeq \frac{N_f\left(N_c^2-1\right)g^4m_\Upsilon k_{10}}{2(2\pi)^5N_cd_\Upsilon d_q|Q\cdot K_1|}\int d^3\boldsymbol{k}\int d^3\boldsymbol{p}_1\delta(q_0+k_{10}-k_{20}-p_{10}-p_{20})|\nabla\psi(\boldsymbol{p})|^2\frac{k^2}{\left(k^2+m_D^2\right)^2}\left(2-\frac{k^2}{2k_1^2}\right). \tag{18}$$

Second, we introduce a dummy variable ω,

$$\delta(q_0+k_{10}-k_{20}-p_{10}-p_{20}) = \int d\omega\delta(\omega+q_0-p_{10}-p_{20})\delta(\omega-k_{10}+k_{20}), \tag{19}$$

and the $\boldsymbol{k}$-$\boldsymbol{p}_1$ phase space is integrated over k, p_1, θ_{kk_1}, θ_{kp_1}, and $\phi_{k;k_1p_1}$, where $\theta_{kk_1}(\theta_{kp_1})$ is the angle between two vectors $\boldsymbol{k}$ and $\boldsymbol{k}_1(\boldsymbol{p}_1)$ and $\phi_{k;k_1p_1}$ is the angle between the $\boldsymbol{k}$-$\boldsymbol{k}_1$ plane and the $\boldsymbol{k}$-$\boldsymbol{p}_1$ plane. For dissolution of weakly bound quarkonia with $\boldsymbol{q} \sim \boldsymbol{p}_1$, $\boldsymbol{p}_2 \gg \boldsymbol{k}$, we use the following relations:

$$\delta(\omega+q_0-p_{10}-p_{20}) \simeq \frac{p_{10}}{kp_1}\delta\left(\cos\theta_{kp_1}-\frac{\omega p_{10}}{kp_1}\right),\quad \delta(\omega-k_{10}+k_{20}) = \frac{k_2}{kk_1}\delta\left(\cos\theta_{kk_1}-\frac{\omega}{k}-\frac{k^2-\omega^2}{2kk_1}\right), \tag{20}$$

to perform the integrations over two polar angles. Then the cross section becomes

$$\sigma^{(q,\bar{q})}_{\rm NLO}(k_1) \simeq \frac{N_f\left(N_c^2-1\right)g^4m_\Upsilon k_{10}}{(2\pi)^3N_cd_\Upsilon d_q|Q\cdot K_1|}\int_0^{2k_1}dk\int dp_1p_1^2|\nabla\psi(\boldsymbol{p})|^2\frac{k^3}{\left(k^2+m_D^2\right)^2}\left(2-\frac{k^2}{2k_1^2}\right), \tag{21}$$

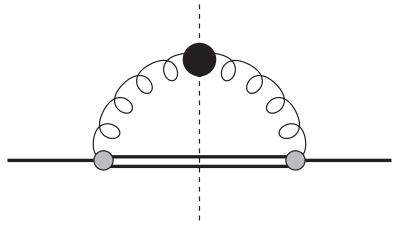

FIG. 4. The self-energy diagram of the quarkonium color singlet. At two-loop order, the cut diagram corresponds to the scattering processes of Fig. 3.

where ω has been integrated over the range $(-\frac{kp_1}{p_{10}}, \frac{kp_1}{p_{10}})$. Finally, in the quarkonium rest frame ($\boldsymbol{q} = 0$), p_1 integration is changed to p^2 integration for a bound state with $|\nabla\psi(\boldsymbol{p})|^2$ as a function of p^2. After integrating over p^2 and k, we obtain

$$\sigma_{\rm NLO}^{(q,\bar{q})}(k_1) \simeq \frac{3N_f\left(N_c^2-1\right)g^4a_0^2}{4N_c d_\Upsilon d_q \pi}\left[\ln\left(\frac{4k_1^2}{m_D^2}\right)-2\right]. \quad (22)$$

Here, we have used the Coulombic bound state Eq. (4), but the relation $a_0^2 = 1/(mE)$ need not be satisfied in general. Similarly, the gluon-quarkonium scattering cross section is determined as

$$\sigma_{\rm NLO}^{(g)}(k_1) \simeq \frac{3\left(N_c^2-1\right)g^4a_0^2}{4d_\Upsilon d_g \pi}\left[\ln\left(\frac{4k_1^2}{m_D^2}\right)-2\right]. \quad (23)$$

In comparison with the leading-order result in Eq. (5), Eqs. (22) and (23) correspond to the dissociation cross sections at next-to-leading order. After multiplying by d_p, they agree with the pNRQCD results for the $mv \gg T \gg m_D \gg E$ regime where inelastic parton scattering is dominant in the effective-field theory framework [11]. In pNRQCD, the NLO results are calculated by the imaginary part of the singlet potential which is from the self-energy diagram (see Fig. 4) of the quarkonium color singlet. We note that the cut diagram at two-loop order corresponds to the scattering processes of Fig. 3, and the leading contribution to gluo-dissociation of Fig. 2.

By convoluting the momentum distributions of incoming and outgoing partons, the thermal width by inelastic parton scattering is given by [11]

$$\Gamma_{\rm NLO} = \int \frac{d^3\boldsymbol{k}_1}{(2\pi)^3}\left\{d_q\sigma_{\rm NLO}^{(q,\bar{q})}(k_1)n_F(k_1)[1-n_F(k_1)] + d_g\sigma_{\rm NLO}^{(g)}(k_1)n_B(k_1)[1+n_B(k_1)]\right\}, \quad (24)$$

where $n_B(k_1)$ and $n_F(k_1)$ are the Bose–Einstein and Fermi–Dirac momentum distributions, respectively. For hard ($\sim T$) momentum, the thermal distribution of an initial parton is $n(k_1)$ with $k_{10} \simeq k_1$, and the Bose-enhancement or Pauli-blocking factor of an outgoing parton has been approximated as $1 \pm n(k_2) \simeq 1 \pm n(k_1)$ for small energy transfer.

IV. NUMERICAL RESULTS FOR $\Upsilon(1S)$

In this section, we focus on the weakly bound $\Upsilon(1S)$ and present the numerical results of the dissociation cross sections and thermal widths. Above the phase-transition temperature, the ground state of bottomonium is expected to survive up to $T \sim 600$ MeV and melts at higher temperature [3]. The binding energy of a Coulombic state depends on the coupling constant $E \sim mg^4$, which increases as temperature decreases. To study transitional behavior at the temperature regime $T \sim$ 200–500 MeV, we set the effective coupling constant $\alpha_s =$ 0.3–0.4 and use the temperature-dependent binding energy which has been estimated in lattice QCD [26]. The Debye screening mass given by $m_D^2 = \frac{g^2T^2}{3}(N_c + \frac{N_f}{2})$ is reduced with time as the temperature decreases with the evolution of quark-gluon plasma after heavy-ion collisions. Although our analysis is based on a Coulombic bound state, the binding energy estimated from nonperturbative lattice computations might allow potential effects which are compatible with lattice QCD findings at short distance. By employing the temperature-dependent binding energy and screening mass, we simulate the running coupling which results $m_D \ll \pi T$ ($m_D \sim \pi T$) for weak (strong) coupling. With $N_c = N_f = 3$, $m = 4.8$ GeV and $a_0 = 0.14$–0.18 fm are used for $\Upsilon(1S)$.

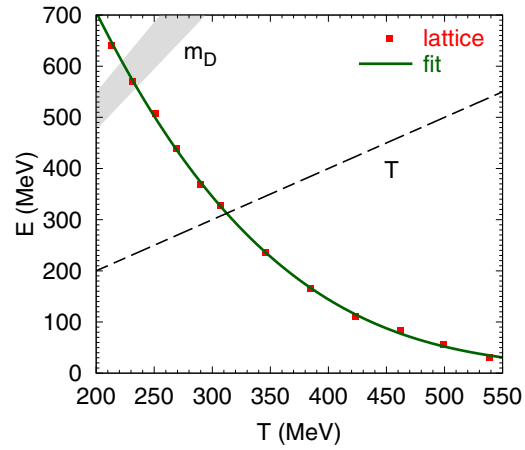

FIG. 5. The binding energy of $\Upsilon(1S)$ from lattice computations [26] and the numerical fit. The black dashed line shows the temperature for reference and the gray band is for the Debye mass as a function of temperature.

Figure 5 shows an upper limit of the binding energy of $\Upsilon(1S)$ computed in lattice QCD [26] and its numerical fit. While the Coulombic binding energy is determined as 243–432 MeV for fixed coupling $\alpha_s = 0.3$–0.4, the binding energy estimated from the lattice QCD decreases as temperature increases. The black dashed line represents the temperature ($E = T$) line, and the gray band is for the Debye mass as a function of T.

Gluo-dissociation is the main mechanism for quarkonium dissolution at low temperature near the phase transition where the binding energy is relatively large. When an incoming gluon carries low momentum, gluo-dissociation contributes up to next-to-leading order. In Fig. 6, we present the dissociation cross sections and the thermal widths at leading [Eq. (5)] and next-to-leading [Eq. (13)] orders. The next-to-leading-order results are slightly smaller than the leading ones. Since the difference is relatively insignificant compared with that from inelastic parton scattering, we consider only leading order for gluo-dissociation in the following.

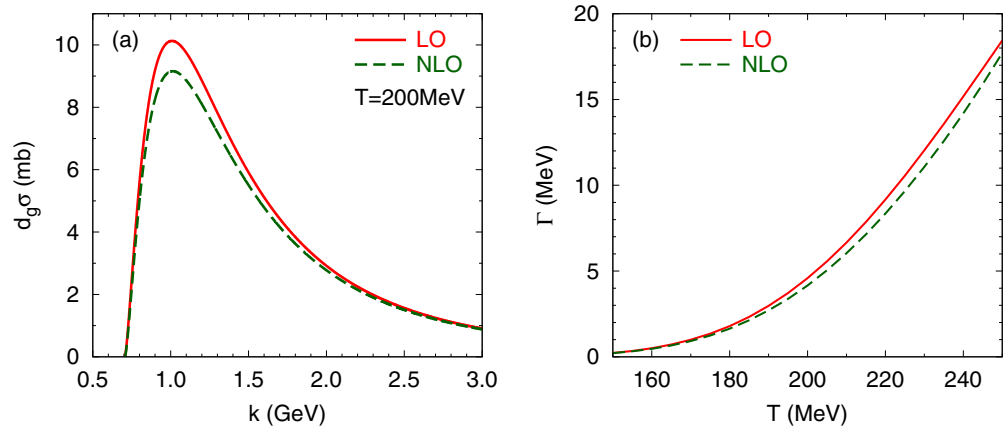

FIG. 6. The leading-order and next-to-leading-order results by gluo-dissociation $[g + \Upsilon(1S) \to b + \bar{b}]$ for $\alpha_s = 0.4$. (a) $\Upsilon(1S)$ dissociation cross sections and (b) thermal widths.

Inelastic parton scattering is important at the high-temperature regime where the binding energy is smaller than T [2]. At high temperature, the Debye mass is large and the logarithmic formula in Eqs. (22) and (23) are not appropriate to study quarkonium dissociation. The cross sections become negative when an incoming parton has low momentum, which does not make sense (see the red solid line in Fig. 7). They are also independent of the binding energy. These are because many restrictions are required to yield the logarithmic formula in the previous section. To obtain phenomenologically acceptable cross sections that can be used throughout a wide temperature region, we integrate the matrix elements of Eq. (16) over the phase space numerically. Since the matrix elements squared are functions of k_1, k_2, and the angle $(\theta_{k_1k_2})$ between $\boldsymbol{k}_1$ and $\boldsymbol{k}_2$, integrating over the energy transfer $(k_0 = k_1 - k_2)$ and $\cos\theta_{k_1k_2}$ yields the cross section as a function of k_1,

$$\sigma_{\rm NLO}(k_1) = \frac{1}{2^5(2\pi)^3 d_\Upsilon d_p m_\Upsilon m k_1} \int_E^{k_1} dk_0 (k_1 - k_0) \times \int d(\cos\theta_{k_1k_2}) p |\mathcal{M}|^2_{\rm NLO}\Big|_{p^2=m(k_0-E)}. \quad (25)$$

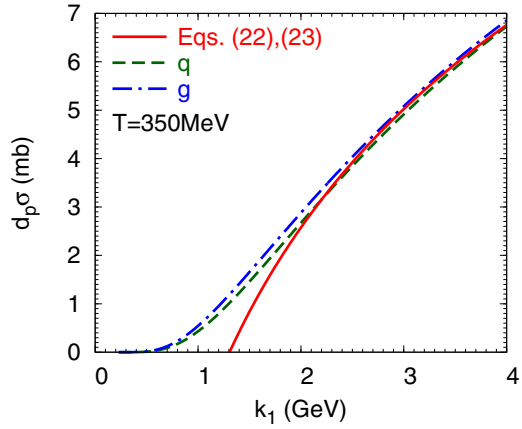

FIG. 7. The comparison of the numerically calculated cross section with the asymptotic formula for $p + \Upsilon(1S) \to p + b + \bar{b}$ with $\alpha_s = 0.4$.

The numerically calculated cross sections are shown in Fig. 7 and compared with the analytical result. The cross sections vary from zero at $k_1 = E$ and smoothly approach the asymptotic formula at high momentum. This method improves the cross sections in the near-threshold region.

In Fig. 8, we present the cross sections of two mechanisms as a function of incoming parton momentum for two different temperatures. Gluo-dissociation is dominant at low momentum, while inelastic parton scattering is important when an incoming parton is energetic. The maximum of the gluo-dissociation cross section depends on the binding energy and shifts to lower momentum as temperature increases. In inelastic parton scattering, the cross section is smaller for higher temperature because the Debye screening mass increases with T.

Figure 9(a) shows the temperature dependence of the thermal width for each mechanism. As temperature decreases during the time evolution, the cross section of gluo-dissociation peaks at higher momentum. In the meanwhile, the phase-space distribution $k^2 n_B(k)$ becomes smaller but peaks at lower momentum close to the maximum of the cross section. As a result, the thermal width by gluo-dissociation increases with

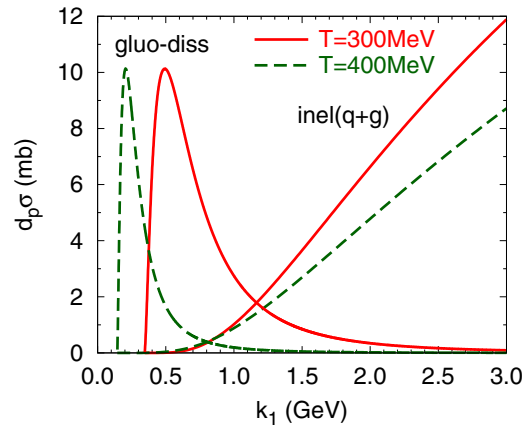

FIG. 8. $\Upsilon(1S)$ dissociation cross sections by gluo-dissociation and inelastic parton scattering for $T = 300,\ 400$ MeV and $\alpha_s = 0.4$.

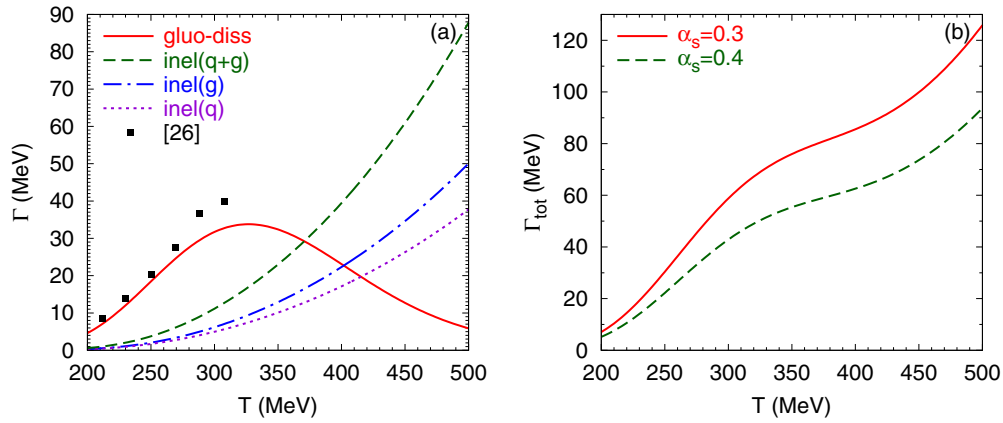

FIG. 9. (a) Temperature dependence of the $\Upsilon(1S)$ thermal widths by gluo-dissociation and inelastic parton scattering for $\alpha_s = 0.4$. (b) The total thermal width as the sum of the contributions by two mechanisms for $\alpha_s = 0.3,\ 0.4$.

time initially but decreases later at low temperature near the phase transition. This behavior seems to contrast with the leading result of Ref. [15] in which the thermal width is proportional to T, but the width in pNRQCD is calculated with the Coulombic binding energy (much smaller than the temperature scale) which is different from the binding energy of Fig. 5. On the other hand, the thermal width by inelastic parton scattering decreases as a collision system cools down, as expected in Ref. [12]. The reason is that, although the cross section at lower temperature is larger, the phase-space distribution $k_1^2 n(k_1)[1 \pm n(k_1)]$ becomes much smaller (and peaks at lower momentum for inelastic quark scattering).

Our numerical results indicate that the dominant mechanism of quarkonium dissociation changes from inelastic parton scattering at high temperature (where $E < T$) to gluo-dissociation near the phase transition (where $E > T$). This transitional behavior depending on temperature is consistent with earlier analyses performed in the quasifree approximation [2,9]. The black squares in Fig. 9(a) represent the width (extracted from Ref. [26]) which is estimated nonperturbatively by tunnelling and direct thermal activation to the continuum in the limit of $E \gg T$ [27]. They are almost same as the width by gluo-dissociation near the phase transition and comparable with the sum of those by two mechanisms at higher temperature.

Figure 9(b) presents the total thermal width as the sum of the contributions by gluo-dissociation and inelastic parton scattering. Because the temperature dependence of inelastic parton scattering is stronger than that of gluo-dissociation, the total width increases with T. At high enough temperature where the thermal width exceeds the binding energy ($\Gamma_{\rm tot} \gtrsim E$), a heavy-quark–antiquark pair is more likely to decay than to be bound so dissociation is expected [3,26]. The weaker the coupling, the larger width we obtain because a smaller screening mass (larger Bohr radius) renders dissociation by inelastic parton scattering (gluo-dissociation) more probable. If we fix the screening mass as $m_D \sim 600$ MeV, the thermal width of inelastic parton scattering increases more rapidly with T. We have checked that varying the parameters does not change significantly the qualitative behavior of the cross sections and thermal widths. Our results agree fairly well with the old calculations in Ref. [28].

V. HIGHER-ORDER CORRECTIONS FOR THERMAL WIDTH

In Sec. III, we obtained the next-to-leading-order contributions to quarkonium dissociation by using the effective vertex derived from the leading-order processes. If we ignore corrections to the effective vertex due to the heavy quark-antiquark interactions, higher-order expansions might be possible. In the perspective of hard thermal loop (HTL) perturbation theory, the external partons are hard ($K_1,\ K_2 \sim T$) and the exchange momentum is soft ($K \sim gT$) in inelastic parton scattering. If all the gluons in Fig. 3(b) are soft, $O(g)$ corrections arise because of the Bose enhancement effects [29].

Another source of $O(g)$ corrections is the diagram in Fig. 10 (and the same except P_1, P_2 exchanged) with soft gluons. The scattering amplitude is given by [21]

$$\mathcal{M}^{\mu\nu\lambda}_{O(g)} = g\frac{g^{\lambda 0}}{k_{20}}\bar{u}(P_1)V_0^{\nu\mu}(k_1)[T^a, T^b]v(P_2), \tag{26}$$

where $V_0^{\nu\mu}(K_1)$ is same as $V^{\nu\mu}(K_1)$ without T^a. As in Sec. III, only the longitudinal gluon part of the effective vertex contributes. By comparing Eqs. (15) and (26), we note that

$$\frac{|\mathcal{M}_{O(g)}|^2}{|\mathcal{M}^{(g)}_{\rm NLO}|^2} \sim \frac{k^2}{k_1^2}. \tag{27}$$

When the external gluons are hard, the process of Fig. 10 is $O(g^2)$ suppressed than the inelastic parton scattering of Fig. 3, which gives the thermal width $\Gamma_{\rm NLO} \sim \int d^3\boldsymbol{k}_1 \sigma_{\rm NLO}(k_1) n(k_1)[1 \pm n(k_1)] \sim g^4 a_0^2 T^3$ [ignoring $\ln(1/g)$] for $k_1 \sim T$. However, if the gluons are soft, the two matrix elements yield the same order of magnitude. Because

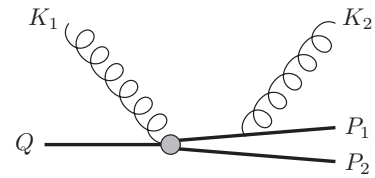

FIG. 10. With soft gluons, $O(g)$ corrections to the next-to-leading order thermal width can be obtained.

$n_B(k_1) \simeq T/k_1 \sim 1/g$ for $k_1 \sim gT$, both Fig. 3(b) and Fig. 10 receive the thermal width of order $g^5 a_0^2 T^3$. These $O(g)$ corrections to $\Gamma_{\rm NLO}$ have been calculated to obtain the momentum diffusion coefficient of a heavy quark at next-to-leading order [22,23].

The momentum diffusion coefficient of a heavy quark is defined as the mean-squared momentum transfer per unit time. At leading order, it is given by [25]

$$3\kappa_{\rm LO} = \frac{1}{2m}\int \frac{d^3\boldsymbol{k}_1}{(2\pi)^3 2k_{10}} \int \frac{d^3\boldsymbol{k}_2}{(2\pi)^3 2k_{20}} \int \frac{d^3\boldsymbol{p}_2}{(2\pi)^3 2p_{20}} \times (2\pi)^4\delta^4(K_1 + P_1 - K_2 - P_2) \times (\boldsymbol{p}_2 - \boldsymbol{p}_1)^2 |\mathcal{M}|^{2(\kappa)}_{\rm LO} n(k_1)[1 \pm n(k_1)], \tag{28}$$

where $\mathcal{M}^{(\kappa)}_{\rm LO}$ is the matrix element for $K_1 + P_1 \to K_2 + P_2$. The corresponding scattering processes are similar to those of Fig. 3 with $K_1,\ K_2 \sim T$. Instead of barely bound quarkonium breaking into a heavy quark and antiquark, a nonrelativistic heavy quark scatters with bath particles exchanging soft momentum. The factor $(\boldsymbol{p}_2 - \boldsymbol{p}_1)^2$ in Eq. (28) corresponds to the momentum transfer $(\boldsymbol{k}_1 - \boldsymbol{k}_2)^2$ in Eq. (16) which comes from the longitudinal gluon part of the effective vertex. By noting that the thermal width has one more momentum integration with a bound state, we obtain the following correspondence [30]:

$$\Gamma_{\rm NLO} \simeq \langle r^2 \rangle \kappa_{\rm LO}, \tag{29}$$

where $\langle r^2 \rangle = \int \frac{d^3\boldsymbol{p}}{(2\pi)^3} |\nabla\psi(\boldsymbol{p})|^2 = 3a_0^2$ for the Coulombic wave function of Eq. (4). If $K_1,\ K_2 \sim gT$, it is plausible to extend the correspondence to the next order, and $\kappa_{\rm NLO}$ in Refs. [22,23] might be useful to obtain $O(g)$ corrections to the thermal width $\Gamma_{\rm NLO}$ [11]. However, because there could be other corrections such as those induced by the heavy-quark-antiquark interactions, we do not proceed further in this work. A recent work Ref. [31] presents a related study on quarkonium dissociation and diffusion based on the potential nonrelativistic QCD.

VI. SUMMARY

We have introduced a partonic picture for quarkonium dissociation that reduces to the formal limit of effective-field theory calculations at the relevant kinematical regime, but that can also be employed in a wide temperature range which is applicable to heavy-quark systems in evolving plasmas. In particular, we have discussed two mechanisms of quarkonium dissociation: gluo-dissociation and inelastic parton scattering, in the limit of small energy transfer which is suitable for weakly bound quarkonia.

Gluo-dissociation is related to the plasmon pole contribution, and inelastic parton scattering is induced by the Landau damping phenomenon. By using hard thermal loop perturbative theory, we have rederived the dissociation cross sections and calculated the thermal widths. The thermal effects at next-to-leading order are obtained through the gluon dispersion relation and resummed propagator for gluo-dissociation and inelastic parton scattering, respectively. Our results in Eqs. (13), (22), and (23) agree with those obtained by potential nonrelativistic QCD in which the thermal width is calculated from the imaginary part of the singlet potential. This might imply that the imaginary parts of the heavy-quark-antiquark potential responsible for quarkonium dissociation basically originate from various scattering processes in thermal medium, at least for weakly bound quarkonia. By comparing with the momentum diffusion coefficient of a heavy quark, we have discussed possible $O(g)$ corrections to the next-to-leading order thermal width.

To study the transitional behavior with the running coupling effects, we have employed the nonperturbative lattice input of binding energy in the analysis of $\Upsilon(1S)$ dissolution. As discussed in the quasifree approximation [2,9], gluo-dissociation is important at low temperature near the phase transition while inelastic parton scattering becomes dominant at high temperature when an incoming parton carries large momentum. Our numerical approach might be useful for phenomenological studies of quarkonia transport in relativistic heavy-ion collisions.

ACKNOWLEDGMENTS

This work is supported by the National Research Foundation of Korea (NRF) grant funded by the Korea government (MSIT) (No. 2018R1C1B6008119 and No. 2016R1D1A1B03930089).

[1] T. Matsui and H. Satz, Phys. Lett. B **178**, 416 (1986).
[2] R. Rapp, D. Blaschke, and P. Crochet, Prog. Part. Nucl. Phys. **65**, 209 (2010).
[3] A. Mocsy, P. Petreczky, and M. Strickland, Int. J. Mod. Phys. A **28**, 1340012 (2013).
[4] S. Chatrchyan *et al.* (CMS Collaboration), Phys. Rev. Lett. **109**, 222301 (2012).
[5] A. M. Sirunyan *et al.* (CMS Collaboration), Phys. Lett. B **790**, 270 (2019).
[6] L. Adamczyk *et al.* (STAR Collaboration), Phys. Rev. C **94**, 064904 (2016).
[7] M. E. Peskin, Nucl. Phys. B **156**, 365 (1979).
[8] G. Bhanot and M. E. Peskin, Nucl. Phys. B **156**, 391 (1979).
[9] L. Grandchamp and R. Rapp, Phys. Lett. B **523**, 60 (2001).
[10] T. Song, W. Park, and S. H. Lee, Phys. Rev. C **81**, 034914 (2010).
[11] N. Brambilla, M. A. Escobedo, J. Ghiglieri, and A. Vairo, J. High Energy Phys. 05 (2013) 130.
[12] M. Laine, O. Philipsen, M. Tassler, and P. Romatschke, J. High Energy Phys. 03 (2007) 054.
[13] N. Brambilla, J. Ghiglieri, A. Vairo, and P. Petreczky, Phys. Rev. D **78**, 014017 (2008).
[14] N. Brambilla, M. A. Escobedo, J. Ghiglieri, J. Soto, and A. Vairo, J. High Energy Phys. 09 (2010) 038.
[15] N. Brambilla, M. A. Escobedo, J. Ghiglieri, and A. Vairo, J. High Energy Phys. 12 (2011) 116.
[16] Y. Oh, S. Kim, and S. H. Lee, Phys. Rev. C **65**, 067901 (2002).

[17] R. L. Kobes and G. W. Semenoff, Nucl. Phys. B **260**, 714 (1985).
[18] R. L. Kobes and G. W. Semenoff, Nucl. Phys. B **272**, 329 (1986).
[19] H. A. Weldon, Phys. Rev. D **28**, 2007 (1983).
[20] H. A. Weldon, Phys. Rev. D **26**, 1394 (1982).
[21] T. Song and S. H. Lee, Phys. Rev. D **72**, 034002 (2005).
[22] S. Caron-Huot and G. D. Moore, Phys. Rev. Lett. **100**, 052301 (2008).
[23] S. Caron-Huot and G. D. Moore, J. High Energy Phys. 02 (2008) 081.
[24] P. Arnold, G. D. Moore, and L. G. Yaffe, J. High Energy Phys. 11 (2000) 001.
[25] G. D. Moore and D. Teaney, Phys. Rev. C **71**, 064904 (2005).
[26] A. Mocsy and P. Petreczky, Phys. Rev. Lett. **99**, 211602 (2007).
[27] D. Kharzeev, L. D. McLerran, and H. Satz, Phys. Lett. B **356**, 349 (1995).
[28] Y. Park, K.-I. Kim, T. Song, S. H. Lee, and C. Y. Wong, Phys. Rev. C **76**, 044907 (2007).
[29] E. Braaten and R. D. Pisarski, Nucl. Phys. B **337**, 569 (1990).
[30] N. Brambilla, M. A. Escobedo, J. Soto, and A. Vairo, Phys. Rev. D **96**, 034021 (2017).
[31] X. Yao and B. Müller, arXiv:1811.09644.